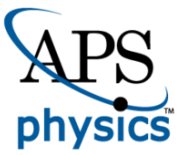

Decoherence-Induced Exceptional Points in a Dissipative Superconducting Qubit

Weijian Chen, Maryam Abbasi, Byung Ha, Serra Erdamar, Yogesh N. Joglekar, and Kater W. Murch

Phys. Rev. Lett. **128**, 110402 — Published 17 March 2022

DOI: 10.1103/PhysRevLett.128.110402

Decoherence Induced Exceptional Points in a Dissipative Superconducting Qubit

Weijian Chen,[1,2,*] Maryam Abbasi,[1] Byung Ha,[1] Serra Erdamar,[1] Yogesh N. Joglekar,[3] and Kater W. Murch[1,2,†]

[1] *Department of Physics, Washington University, St. Louis, MO, USA, 63130*
[2] *Center for Quantum Sensors, Washington University, St. Louis, MO, USA, 63130*
[3] *Department of Physics, Indiana University-Purdue University Indianapolis, Indianapolis, IN, USA, 46202*

(Dated: February 16, 2022)

Open quantum systems interacting with an environment exhibit dynamics described by the combination of dissipation and coherent Hamiltonian evolution. Taken together, these effects are captured by a Liouvillian superoperator. The degeneracies of the (generically non-Hermitian) Liouvillian are exceptional points, which are associated with critical dynamics as the system approaches steady state. We use a superconducting transmon circuit coupled to an engineered environment to observe two different types of Liouvillian exceptional points that arise either from the interplay of energy loss and decoherence or purely due to decoherence. By dynamically tuning the Liouvillian superoperators in real time we observe a non-Hermiticity-induced chiral state transfer. Our study motivates a new look at open quantum system dynamics from the vantage of Liouvillian exceptional points, enabling applications of non-Hermitian dynamics in the understanding and control of open quantum system.

Exceptional points degeneracies (EPs) have been extensively studied in classical dissipative systems with energy or particle loss where the dynamics are governed by effective non-Hermitian Hamiltonians [1, 2]. Recently, there is growing interest to harness non-Hermiticities for quantum applications ranging from sensing [3–5] to state control [6, 7]. Various approaches have been used to implement non-Hermitian Hamiltonians in quantum systems such as introducing a mode-selective loss [8, 9], embedding the desired non-Hermitian Hamiltonian into a larger Hermitian system [6, 10], or removing quantum jumps from the evolution of an open quantum system through postselection [7, 11]. However, despite its essential role in quantum systems, decoherence has not been a focus of these studies. Indeed, decoherence and its effects cannot be captured by an effective non-Hermitian Hamiltonian formalism. Liouvillian superoperators have been proposed to take account of both the energy loss and decoherence, capturing the full dynamics of a decohering non-Hermitian system [12–17]. In the Liouvillian formalism, the dissipative effects are captured by Lindblad dissipators, whose effects come in two parts: one is a coherent nonunitary evolution (i.e., energy or particle loss) and the other is quantum jumps between the energy levels that lead to decoherence [18, 19]. This formalism provides a critical examination when generalizing phenomena and applications observed in classical systems to quantum systems such as EP sensors [20–22]. The Liouvillian superoperators also exhibit EPs, termed as Liouvillian EPs (LEPs), to differentiate from those EPs obtained from Hamiltonians, but these LEPs and their properties have not yet been experimentally observed. In this Letter, we study the transient dynamics of a dissipative superconducting qubit as it evolves toward its steady state. We observe LEPs that arise from the interplay of energy loss and decoherence. By dynamically tuning the Liouvillian superoperator in real time we observe a non-Hermiticity-induced chiral state transfer. Further, by expanding the dimension of the Hilbert space from two to three, we construct a subspace where the non-Hermiticity is purely due to decoherence. Our study shows the rich features and potential applications of non-Hermitian physics and EPs beyond the Hamiltonian formalism, further enriching applications of open quantum systems in quantum information technology.

The dynamics of a driven dissipative two-level system [Fig. 1(a)] can be described by a Lindblad master equation:

$$\dot{\rho} = -i[H_c, \rho] + \sum_{k=e,\phi} [L_k \rho L_k^\dagger - \frac{1}{2}\{L_k^\dagger L_k, \rho\}] \equiv \mathcal{L}\rho, \quad (1)$$

where ρ denotes the density operator, and $L_{e,\phi}$ are the jump operators, defined as $L_e = \sqrt{\gamma_e}|g\rangle\langle e|$ and $L_\phi = \sqrt{\gamma_\phi/2}\sigma_z$, describing spontaneous emission from level $|e\rangle$ to level $|g\rangle$ at a rate γ_e and pure dephasing at a rate γ_ϕ, respectively. $H_c = J(|g\rangle\langle e| + |e\rangle\langle g|) + \Delta/2(|g\rangle\langle g| - |e\rangle\langle e|)$, characterizes coupling between two levels by a drive with the frequency detuning Δ relative to the $|g\rangle$–$|e\rangle$ transition at a rate J. The dynamics can be fully captured by a Liouvillian superoperator $\mathcal{L}$. Given a Hilbert space of dimension N, the Liouvillian approach is based on representation of the system state as a density operator and the corresponding Liouville space has a dimension of N^2. The four eigenvalues of the Liouvillian superoperator are provided in Fig. 1(b,c) for $\Delta = 0$: two of them are real numbers, and the other two exhibit a second-order LEP degeneracy at $J_{\rm LEP} = \gamma_e/8 - \gamma_\phi/4$ with a transition from real to complex numbers.

Physical intuition for this LEP can be obtained by recasting the Lindblad equation into a Bloch equation for the expectation values of the Pauli operators $\{x, y, z\} \equiv$

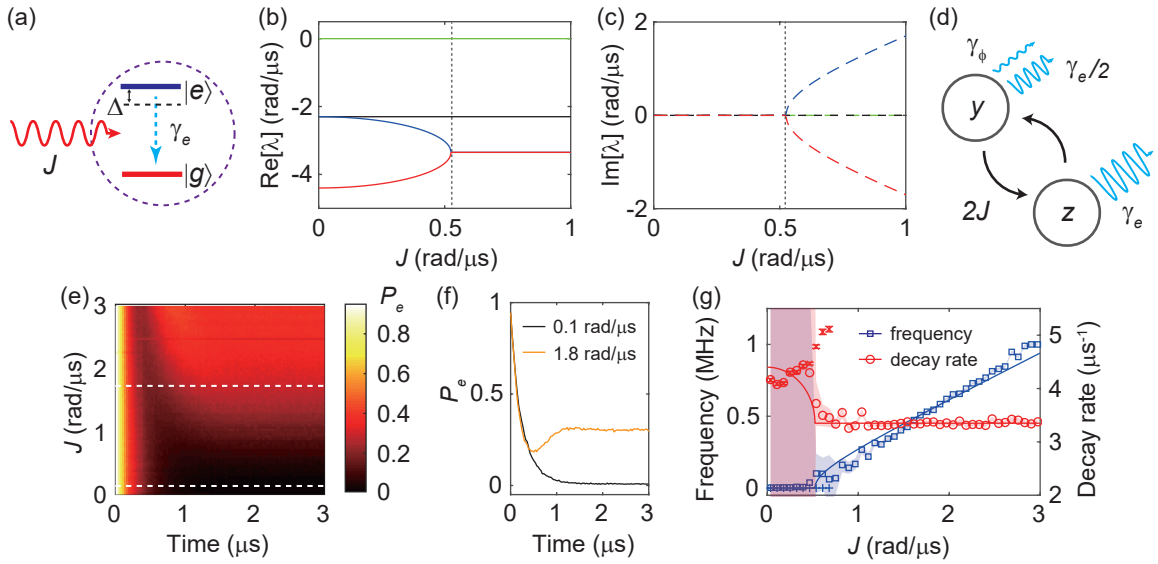

FIG. 1. **Liouvillian EP in the dynamics of a driven dissipative qubit.** (a) Schematic of the system; γ_e denotes the spontaneous emission rate of the $|e\rangle$ level, and J denotes the coupling rate from an applied drive with frequency detuning Δ relative to the $|g\rangle$–$|e\rangle$ transition. (b-c) Real (solid curves) and imaginary (dashed curves) parts of the Liouvillian spectra when $\Delta = 0$; the LEP is indicated with a vertical dashed line. The parameters used for calculations are: $\gamma_e = 4.4\,\mu\text{s}^{-1}$ and $\gamma_\phi = 0.1\,\mu\text{s}^{-1}$. (d) The coupling between the Pauli expectation values y and z with different losses can be viewed in terms of a two-mode system (y, z) with passive PT symmetry and EPs. (e) Population dynamics versus evolution time at different J values with the qubit initialized at the $|e\rangle$ state. Two examples (marked by the white dashed lines) of population evolution at $J = 0.1\,\text{rad}\,\mu\text{s}^{-1}$ (black curve) and $J = 1.8\,\text{rad}\,\mu\text{s}^{-1}$ (orange curve) are shown in (f). (g) Oscillation frequency (blue squares) and decay rate (red circles) at different drive amplitudes; the transition marks a LEP. The shaded areas represent the standard error of the oscillation frequency (blue) and decay rate (red) from fitting the qubit dynamics to a decaying sine wave. The fitting error diverges below the LEP. The corresponding data are also processed by fitting to exponential decay, and the obtained decay rates (red crosses) and frequencies (fixed to zero, blue plus symbols) and error bars are provided for comparison. The solid curves are calculated from the Liouvillian spectra, where the dissipation rates $\gamma_e = 4.4\,\mu\text{s}^{-1}$ and $\gamma_\phi = 0.1\,\mu\text{s}^{-1}$ are used.

$\{\langle\sigma_x\rangle, \langle\sigma_y\rangle, \langle\sigma_z\rangle\}$ [23],

$$\begin{pmatrix}\dot{x}\\ \dot{y}\\ \dot{z}\end{pmatrix} = -\begin{pmatrix}\frac{\gamma_e}{2}+\gamma_\phi & \Delta & 0\\ -\Delta & \frac{\gamma_e}{2}+\gamma_\phi & 2J\\ 0 & -2J & \gamma_e\end{pmatrix}\begin{pmatrix}x\\ y\\ z\end{pmatrix} + \begin{pmatrix}0\\ 0\\ \gamma_e\end{pmatrix}. \quad (2)$$

The y and z components are coupled, yet exhibit different losses, yielding effectively a passive parity-time (PT) symmetric system [Fig. 1(d)]. The z component exhibits a loss of excitation (energy), whereas the y component exhibits decoherence from both spontaneous emission and pure dephasing. There is one LEP for $\Delta = 0$ except when $\gamma_e = 2\gamma_\phi$, where the loss rates for y and z are the same.

In the experiment, we use the lowest two energy levels ($|g\rangle$, $|e\rangle$) of a transmon superconducting circuit [24]. The transmon is dispersively coupled to a three-dimensional microwave cavity, leading to a state-dependent cavity resonance frequency. High fidelity, single-shot readout of the transmon state can be realized by probing the cavity with a weak microwave signal and detecting its phase shift [25]. Further, we shape the density of states of the electromagnetic field which allows us to adjust the dissipation rate of the energy level $|e\rangle$ [11]. In this study, we set $\gamma_e \approx 4.5\,\mu\text{s}^{-1}$, much greater than the pure dephasing rate $\gamma_\phi \approx 0.2\,\mu\text{s}^{-1}$ so that there is a large difference between the losses of y and z.

To experimentally identify the LEP, we study the transient dynamics of the qubit to its steady state. We initialize the qubit in the $|e\rangle$ state and then apply a resonant microwave drive to induce a coupling at rate J. Figure 1(e) displays the measured evolution of the $|e\rangle$ state population for different J. We observe a transition from exponential decay to exponentially damped oscillation as the coupling rate is increased. Examples of the evolution at two different drive amplitudes above and below the LEP are shown in Fig. 1(f). A classical analogy of this observation is a damped harmonic oscillator, where a second-order EP (corresponding to critical damping) marks the transition from an overdamped to an underdamped regime. The results are processed by fitting to a decaying sine wave to determine the oscillation frequency and decay rate [Fig. 1(g)], which show a transition at $J \simeq \gamma_e/8$, in agreement with the Liouvillian eigenvalues. The fitting uncertainty [the shaded areas in Fig. 1(g)] diverges when near or below the LEP, which we attribute to the redundant free parameters for a decaying sine curve. We further inspect those data by fitting them to simple exponential decay: the obtained decay rates match with those obtained from fitting to decaying sine wave and

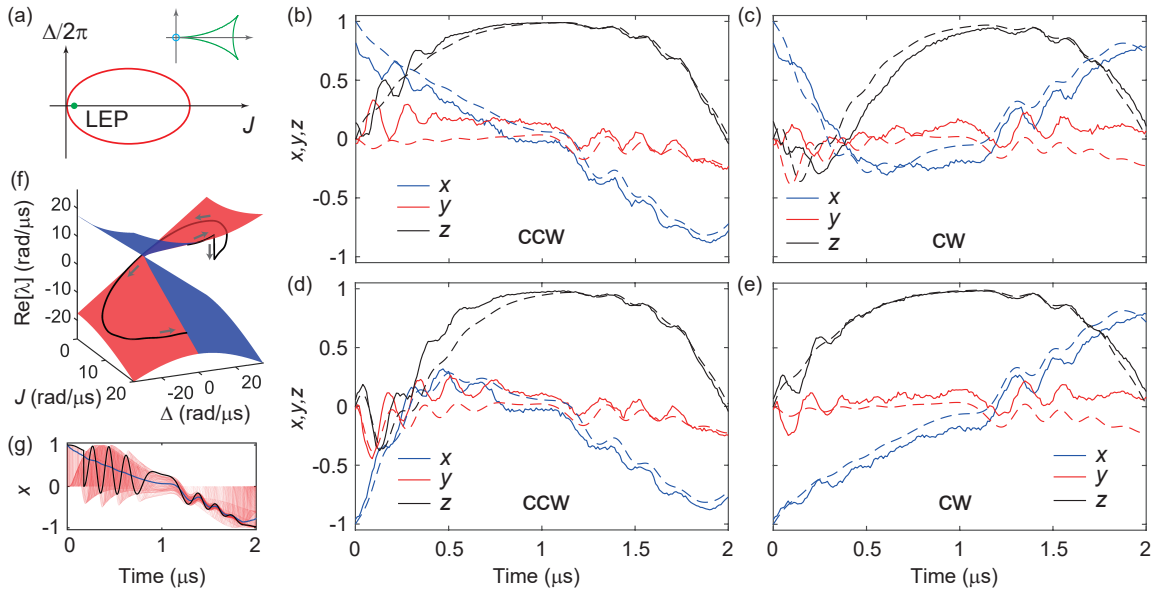

FIG. 2. **Dynamical encircling of the Liouvillian EP structure.** (a) Schematic of the parameter path (red ellipse) that encircles a LEP structure (denoted as a green dot) in the parameter space (J, Δ). The Liouvillian superoperator exhibits second-order exceptional lines, forming a triangle-shaped LEP structure (inset). Note that the LEP structure excludes the origin point ($J = 0$ and $\Delta = 0$), marked by the empty circle in the inset (b-e) Evolution of the Bloch components under two different initial states ($|\pm x\rangle$) and two encircling directions (cw, ccw). The solid curves are the experimental results. We sample 10^4 measurements per point, leading to a standard error of ~ 0.01, similar to the thickness of the plotted lines. The dashed curves are the theoretical calculations from Lindblad master equation, with $\gamma_e = 4.6\,\mu s^{-1}$ and $\gamma_\phi = 0.2\,\mu s^{-1}$. (f) Illustration of one quantum trajectory (marked by grey arrows) on the Riemann surface, where there is one quantum jump (vertical part of the trajectory). This trajectory is one example (black curve) from 1000 simulated trajectories (red curves) shown in (g). The average of the trajectories is the solution of the Lindblad equation (blue curve).

have low uncertainty. We therefore conclude our observation shows the LEP transition.

One signature of Hamiltonian based EPs is the chiral state transfer that occurs when the Hamiltonian parameters are tuned to encircle an EP. As a result of the topological structure of the Riemann manifold that describes the system's complex energy, one state will map to the other after the encirclement. Relative gain or loss along different paths results in chiral state or population transfer [6, 7, 26–28]. This process has also been shown to induce a chiral geometric phase on quantum states [7]. Here, we investigate whether these population features persist when encircling the LEPs in the parameter space (J, Δ).

For non-zero Δ, the Liouvillian exhibits second-order LEP lines and two third-order LEPs, forming a small "LEP structure" very near the LEP for $\Delta = 0$ (inset in Fig. 2(a)) [29]. We now investigate the effects of dynamically tuning the Liouvillian parameters to encircle this LEP structure. We choose a closed parameter path defined as $J(t) = 16\cos^2(\pi t/T)\,\mathrm{rad}\,\mu s^{-1}$ and $\Delta(t) = \pm 10\pi \sin(2\pi t/T)\,\mathrm{rad}\,\mu s^{-1}$, where $T = 2\ \mu s$ is the loop period, and "$+$" and "$-$" correspond to counterclockwise (ccw) and clockwise (cw) encircling directions, respectively [Fig. 2(a)]. We choose the initial state $|+x\rangle$ at $t = 0$. The results of quantum state tomography at different points along the parameter path for both cw and ccw directions are shown in Fig. 2(b, c). While for the ccw direction, the initial state is transferred to a state close to $|-x\rangle$, for the cw direction, the final state remains approximately at $|+x\rangle$. Similar observations also apply to the case with the initial state $|-x\rangle$ [Fig. 2(d,e)]. The deviations of experimental results from theoretical calculations are mainly attributed to readout infidelity, imperfect state preparation, and small errors in the tomography calibration.

This chiral behavior can be understood from a quantum trajectory picture. The qubit evolution can be described by a non-Hermitian Hamiltonian evolution that is interrupted by randomly occurring quantum jumps. The non-Hermitian Hamiltonian evolution pertains to the Riemann structure displayed in Fig. 2(f), which would induce a state transfer upon one encircling. Figure 2(f) displays one such trajectory where a quantum jump occurs. The initial state is $|+x\rangle$, and a jump to $|g\rangle$ occurs shortly after the beginning of the parameter sweep (at $t \simeq 0.2\ \mu s$), bringing x abruptly to zero. This state continues to evolve under the time dependent Hamiltonian. Remarkably, at the end of the parameter sweep, the final state is near $|-x\rangle$. An ensemble of such trajectories is shown in Fig. 2(g). This chirality of state transfer originates from the directionality of the quantum jumps which

favors the ground state and therefore disappears in the Hermitian limit (see the Supplementary Materials [29]). Additionally, the chirality is relatively insensitive to small changes in the loop parameters, occurring for loops that come near, intersect, or encircle the LEP structure [30].

We highlight several aspects that are different from previous studies of encircling EPs based on non-Hermitian Hamiltonians. First, in previous studies, the initial state is usually chosen to be an eigenstate. However, here the initial states $|\pm x\rangle$ do not directly correspond to the eigenstates of the Liouvillian superoperators; instead, they are approximately a superposition of two Liouvillian eigenstates, one of which corresponds to the steady state, the other an unphysical state [14, 29]. Second, the evolution is trace preserving; in contrast, for the evolution governed by non-Hermitian Hamiltonian [7], the state norm decreases with time, and a state renormalization at each time step is then required. Third, the quantum state is mixed due to the decoherence, which will limit the practical applications of this chiral state transfer protocol. As we show in the Supplementary Materials [29], the decoherence effects can be minimized by optimizing the driving conditions while maintaining the chiral behavior.

So far, we have only focused on the lowest two levels of the transmon circuit. By including a higher energy level (i.e., the $|f\rangle$ level, with spontaneous decay rate $\gamma_f \ll \gamma_e$) as a coherence reference [Fig. 3(a)], we discover a second type of LEP that is fully induced by decoherence and has no energy loss involved. The corresponding Liouville space then has a dimension of 9, and the Liouvillian spectra are provided in the Supplementary Materials [29]. The decoherence induced LEP results from the coupling between two coherences ρ_{gf} and ρ_{ef} of this qutrit and occurs at $J = \gamma_e/4$ [Fig. 3(a)]. The dissipation of the $|e\rangle$ level leads to the loss of the coherence ρ_{ef}, but not the coherence ρ_{gf}. As with energy loss induced EPs, the interplay between coupling and decoherence yields this LEP.

To observe this LEP transition, we initialize the circuit in the state $(|g\rangle - |f\rangle)/\sqrt{2}$ and then apply a resonant drive with variable duration to $\{|g\rangle, |e\rangle\}$ transition, followed by a tomography pulse to determine ρ_{gf} [31, 32]. As displayed in Fig. 3(b), for large J, we observe damped oscillations in ρ_{gf}, yet for $J < 1$ rad/μs the oscillations are replaced with exponential decay. We quantify this transition by fitting the ρ_{gf} evolution to a damped sine wave, extracting the frequency and decay rate as displayed in Fig. 3(c). We note that this decoherence induced LEP is non-local in the sense that it only relies on initial coherence between the $|f\rangle$ and $|g\rangle$ states, but no further coupling between the $\{|f\rangle\}$ and $\{|g\rangle, |e\rangle\}$ manifolds. Therefore, we expect such decoherence induced LEPs to play a critical role in how many-body correlations decay due to local operations and sources of dissipation.

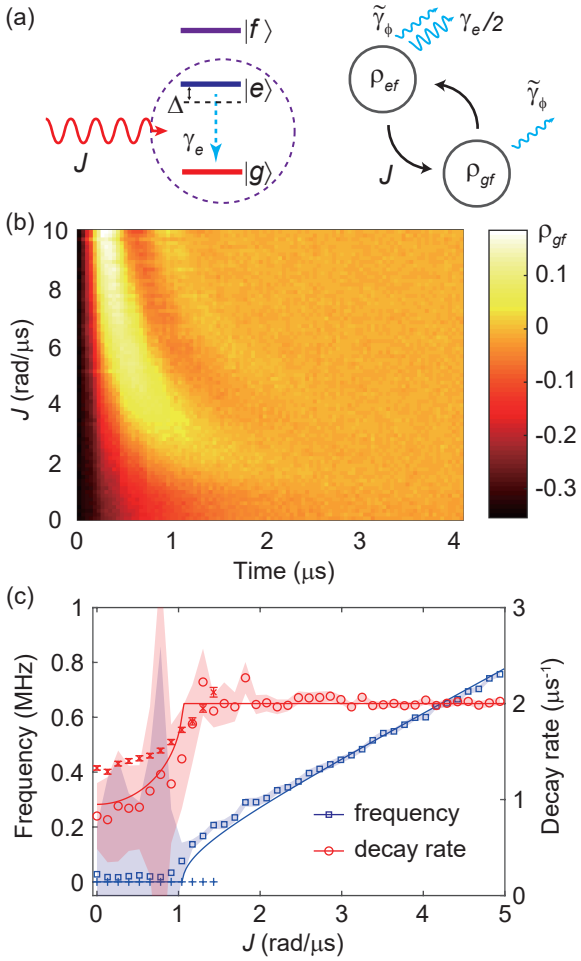

FIG. 3. **Decoherence induced Liouvillian EP.** (a) Schematic of a driven dissipative qutrit. The physical origin of this LEP arises from the coupling between two coherences of the density matrix ρ_{gf} and ρ_{ef} that experience unbalanced losses. The two coherences have the same loss $\tilde{\gamma}_\phi$ from the dissipations of the reference level $|f\rangle$, but ρ_{ef} has additional loss from γ_e. (b) The measured coherence ρ_{gf} versus evolution time at different J values. (c) Oscillation frequency (blue squares) and decay rate (red circles) at different drive amplitudes, where the transition marks a LEP. The bands represent the standard error of the fit. The red crosses and blue plus symbols indicate the results from an exponential fit. The solid curves are calculated from the Liouvillian spectra. Parameters used are $\gamma_e = 4.2\ \mu s^{-1}$, $\gamma_\phi = 0.2\ \mu s^{-1}$, $\gamma_f = 0.3\ \mu s^{-1}$, and an additional overall loss $0.75\ \mu s^{-1}$ is added to account for additional decoherence of the $|f\rangle$ state.

Our study has revealed and quantified two new types of EPs occurring in single dissipative quantum systems. In contrast to prior work, these LEPs do not rely on postselection to induce non-Hermitian dynamics but instead are evident in the transient dynamics of an open quantum system as it approaches steady state. Because the Liouvillian formalism applies to all Markovian dissipative interactions it also encompasses the effects of quantum measurement [33]. For instance, the quantum

Zeno effect pertains to the competition between coherent coupling and the dissipative effects of measurement [34–37]. The transition from a Zeno pinning regime can naturally be treated in the context of LEPs introduced here [38–41]. Our study therefore motivates a new look at open quantum system dynamics from the vantage of Liouvillian exceptional points, enabling applications of non-Hermitian dynamics in Floquet physics [42], quantum steering [43], state transfer [44, 45], measurement induced dynamics [46, 47], and quantum thermal engines [48].

We acknowledge K. Snizhko and P. Kumar for inspiring discussions. This research was supported by NSF Grant No. PHY-1752844 (CAREER), AFOSR MURI Grant No. FA9550-21-1-0202, ONR Grant No. N00014-21-1-2630, and the Institute of Materials Science and Engineering at Washington University.

* wchen34@wustl.edu
† murch@physics.wustl.edu

[1] Miri, M. A. & Alù, A. Exceptional points in optics and photonics. *Science* **363**, 7709 (2019).
[2] Özdemir, S. K., Rotter, S., Nori, F. & Yang, L. Parity-time symmetry and exceptional points in photonics. *Nature Materials* **18**, 783–798 (2019).
[3] Lau, H.-K. & Clerk, A. A. Fundamental limits and non-reciprocal approaches in non-Hermitian quantum sensing. *Nature communications* **9**, 1–13 (2018).
[4] McDonald, A. & Clerk, A. A. Exponentially-enhanced quantum sensing with non-Hermitian lattice dynamics. *Nature communications* **11**, 1–12 (2020).
[5] Yu, S. *et al.* Experimental Investigation of Quantum $\mathcal{PT}$-Enhanced Sensor. *Phys. Rev. Lett.* **125**, 240506 (2020).
[6] Liu, W., Wu, Y., Duan, C.-K., Rong, X. & Du, J. Dynamically Encircling an Exceptional Point in a Real Quantum System. *Phys. Rev. Lett.* **126**, 170506 (2021).
[7] Abbasi, M., Chen, W., Naghiloo, M., Joglekar, Y. N. & Murch, K. W. Topological quantum state control through Floquet exceptional-point proximity (2021). 2108.05365.
[8] Xiao, L. *et al.* Observation of topological edge states in parity time symmetric quantum walks. *Nature Physics* **13**, 1117–1123 (2017).
[9] Klauck, F. *et al.* Observation of PT-symmetric quantum interference. *Nature Photonics* **13**, 883–887 (2019).
[10] Wu, Y. *et al.* Observation of parity-time symmetry breaking in a single-spin system. *Science* **364**, 878–880 (2019).
[11] Naghiloo, M., Abbasi, M., Joglekar, Y. N. & Murch, K. W. Quantum state tomography across the exceptional point in a single dissipative qubit. *Nature Physics* **15**, 1232–1236 (2019).
[12] Mathisen, T. & Larson, J. Liouvillian of the open STIRAP problem. *Entropy* **20**, 20 (2018).
[13] Hatano, N. Exceptional points of the Lindblad operator of a two-level system. *Molecular Physics* **117**, 2121–2127 (2019).
[14] Minganti, F., Miranowicz, A., Chhajlany, R. W. & Nori, F. Quantum exceptional points of non-Hermitian Hamiltonians and Liouvillians: The effects of quantum jumps. *Physical Review A* **100**, 062131 (2019).
[15] Minganti, F., Miranowicz, A., Chhajlany, R. W., Arkhipov, I. I. & Nori, F. Hybrid-Liouvillian formalism connecting exceptional points of non-Hermitian Hamiltonians and Liouvillians via postselection of quantum trajectories. *Phys. Rev. A* **101**, 062112 (2020).
[16] Arkhipov, I. I., Miranowicz, A., Minganti, F. & Nori, F. Quantum and semiclassical exceptional points of a linear system of coupled cavities with losses and gain within the Scully-Lamb laser theory. *Phys. Rev. A* **101**, 013812 (2020).
[17] Chen, W., Abbasi, M., Joglekar, Y. N. & Murch, K. W. Quantum Jumps in the Non-Hermitian Dynamics of a Superconducting Qubit. *Phys. Rev. Lett.* **127**, 140504 (2021).
[18] Dalibard, J., Castin, Y. & Mølmer, K. Wave-function approach to dissipative processes in quantum optics. *Physical Review Letters* **68**, 580–583 (1992).
[19] Plenio, M. B. & Knight, P. L. The quantum-jump approach to dissipative dynamics in quantum optics. *Reviews of Modern Physics* **70**, 101 (1998).
[20] Wiersig, J. Enhancing the Sensitivity of Frequency and Energy Splitting Detection by Using Exceptional Points: Application to Microcavity Sensors for Single-Particle Detection. *Phys. Rev. Lett.* **112**, 203901 (2014).
[21] Chen, W., Özdemir, S. K., Zhao, G., Wiersig, J. & Yang, L. Exceptional points enhance sensing in an optical microcavity. *Nature* **548**, 192–196 (2017).
[22] Wiersig, J. Robustness of exceptional-point-based sensors against parametric noise: The role of Hamiltonian and Liouvillian degeneracies. *Phys. Rev. A* **101**, 053846 (2020).
[23] Am-Shallem, M., Kosloff, R. & Moiseyev, N. Exceptional points for parameter estimation in open quantum systems: Analysis of the Bloch equations. *New Journal of Physics* **17**, 113036 (2015).
[24] Koch, J. *et al.* Charge-insensitive qubit design derived from the Cooper pair box. *Physical Review A* **76**, 042319 (2007).
[25] Wallraff, A. *et al.* Approaching Unit Visibility for Control of a Superconducting Qubit with Dispersive Readout. *Phys. Rev. Lett.* **95**, 060501 (2005).
[26] Xu, H., Mason, D., Jiang, L. & Harris, J. G. Topological energy transfer in an optomechanical system with exceptional points. *Nature* **537**, 80–83 (2016).
[27] Doppler, J. *et al.* Dynamically encircling an exceptional point for asymmetric mode switching. *Nature* **537**, 76–79 (2016).
[28] Choi, Y., Hahn, C., Yoon, J. W., Song, S. H. & Berini, P. Extremely broadband, on-chip optical nonreciprocity enabled by mimicking nonlinear anti-adiabatic quantum jumps near exceptional points. *Nature Communications* **8**, 14154 (2017).
[29] In supplementary materials, we provide more details of our experimental setup, the Liouvillian spectra, and more results for dynamically encircling LEPs.
[30] Hassan, A. U. *et al.* Chiral state conversion without encircling an exceptional point. *Physical Review A* **96**, 052129 (2017).
[31] Thew, R. T., Nemoto, K., White, A. G. & Munro, W. J. Qudit quantum-state tomography. *Phys. Rev. A* **66**, 012303 (2002).
[32] Bianchetti, R. *et al.* Control and Tomography of a Three

Level Superconducting Artificial Atom. *Phys. Rev. Lett.* **105**, 223601 (2010).

[33] de Castro, L. A., de S Neto, O. P. & Brasil, C. A. An introduction to quantum measurements with a historical motivation (2019). 1908.03949.

[34] Presilla, C., Onofrio, R. & Tambini, U. Measurement Quantum Mechanics and Experiments on Quantum Zeno Effect. *Annals of Physics* **248**, 95–121 (1996).

[35] Álvarez, G. A., Danieli, E. P., Levstein, P. R. & Pastawski, H. M. Environmentally induced quantum dynamical phase transition in the spin swapping operation. *The Journal of chemical physics* **124**, 194507 (2006).

[36] Danieli, E. P., Álvarez, G. A., Levstein, P. R. & Pastawski, H. M. Quantum dynamical phase transition in a system with many-body interactions. *Solid state communications* **141**, 422–426 (2007).

[37] Kakuyanagi, K. *et al.* Observation of quantum Zeno effect in a superconducting flux qubit **17**, 063035 (2015).

[38] Kumar, P., Romito, A. & Snizhko, K. Quantum Zeno effect with partial measurement and noisy dynamics. *Phys. Rev. Research* **2**, 043420 (2020).

[39] Chen, T. *et al.* Quantum Zeno effects across a parity-time symmetry breaking transition in atomic momentum space. *npj Quantum Information* **7**, 1–6 (2021).

[40] Li, J., Wang, T., Luo, L., Vemuri, S. & Joglekar, Y. N. Unification of quantum Zeno-anti Zeno effects and parity-time symmetry breaking transitions (2020). 2004.01364.

[41] Popkov, V. & Presilla, C. Full spectrum of the Liouvillian of open dissipative quantum systems in the Zeno limit. *Physical Review Letters* **126**, 190402 (2021).

[42] Gunderson, J., Muldoon, J., Murch, K. W. & Joglekar, Y. N. Floquet exceptional contours in Lindblad dynamics with time-periodic drive and dissipation. *Phys. Rev. A* **103**, 023718 (2021).

[43] Kumar, P., Snizhko, K., Gefen, Y. & Rosenow, B. Optimized steering: Quantum state engineering and exceptional points. *Phys. Rev. A* **105**, L010203 (2022).

[44] Pick, A., Silberstein, S., Moiseyev, N. & Bar-Gill, N. Robust mode conversion in NV centers using exceptional points. *Physical Review Research* **1**, 013015 (2019).

[45] Kumar, P., Snizhko, K. & Gefen, Y. Near-unit efficiency of chiral state conversion via hybrid-Liouvillian dynamics. *Phys. Rev. A* **104**, L050405 (2021).

[46] Hacohen-Gourgy, S., García-Pintos, L. P., Martin, L. S., Dressel, J. & Siddiqi, I. Incoherent Qubit Control Using the Quantum Zeno Effect. *Phys. Rev. Lett.* **120**, 020505 (2018).

[47] Wang, Y., Snizhko, K., Romito, A., Gefen, Y. & Murch, K. Observing a Topological Transition in Weak-Measurement-Induced Geometric Phases (2021). arXiv:2102.05660.

[48] Khandelwal, S., Brunner, N. & Haack, G. Signatures of Liouvillian Exceptional Points in a Quantum Thermal Machine. *PRX Quantum* **2**, 040346 (2021).

[49] Noh, H.-R. & Jhe, W. Analytic solutions of the optical Bloch equations. *Optics Communications* **283**, 2353–2355 (2010).